# **Metals & corrosion**



# Effect of solution treatment temperature upon the microstructure and mechanical properties of hot rolled Inconel 625 alloy

Fei Yang<sup>1</sup> , Liming Dong<sup>1,2</sup>, Xianjun Hu<sup>3</sup>, Xuefeng Zhou<sup>1</sup>, Zonghan Xie<sup>4,5</sup>, and Feng Fang<sup>1,\*</sup>

Received: 2 September 2019
Accepted: 22 January 2020
Published online:

2 February 2020

© Springer Science+Business Media, LLC, part of Springer Nature 2020

### **ABSTRACT**

The influence of solution treatment temperature on the microstructure and mechanical properties of hot rolled Inconel 625 alloy was investigated. The results show that the microstructure of the hot rolled alloy is mainly composed of austenite equiaxed grains, with the secondary phase being dominated by MC carbide rich in Nb and Ti. The alloy possesses a high strength of 959 MPa with a hardness of 262 HV, but modest plasticity with a tensile elongation of 48%. The effects of grain refinement and dislocation entanglement are considered to be the main mechanisms responsible for the excellent strength in the alloy. For the solution treatment temperature set in the range of 950-1050 °C, the average grain size of the treated alloy did not change significantly, and the carbide phase was dissolved slowly. As such, the temperature has little effect on the mechanical properties of the alloy. At the temperature higher than 1150 °C, the carbide was dissolved near the grain boundaries and, at the same time, the grains grew rapidly. Consequently, the tensile strength and hardness of the treated alloy decreased considerably, whereas the elongation to fracture increased from about 47% to more than 60%. The strength-ductility trade-off is attributable to a synergy of grain coarsening, dislocation annihilation and the dissolution of precipitate phase during solid solution treatment. Moreover, the <111> recrystallization texture was observed after solution treatment at higher temperatures.

Address correspondence to E-mail: fangfeng@seu.edu.cn



<sup>&</sup>lt;sup>1</sup> Jiangsu Key Laboratory of Advanced Metallic Materials, School of Materials Science and Engineering, Southeast University, Jiangning District, Nanjing 211189, China

<sup>&</sup>lt;sup>2</sup> School of Automotive Engineering, Changshu Institute of Technology, Changshu 215500, China

<sup>&</sup>lt;sup>3</sup> Jiangsu Sha-Steel Group, Zhangjiagang 215625, China

<sup>&</sup>lt;sup>4</sup>School of Materials and Energy, Southwest University, Chongging 400715, China

<sup>&</sup>lt;sup>5</sup>School of Mechanical Engineering, University of Adelaide, Adelaide, SA 5005, Australia

### Introduction

Inconel 625 alloy (Ni-Cr-Mo-Nb) is a solid solutionstrengthened nickel-based alloy [1]. Because of its excellent mechanical properties and corrosion resistance [2], Inconel 625 alloy has been widely used in gas turbine, nuclear power generation and chemical processing applications, where operating conditions are harsh [3–5]. Due to the high content of refractory elements such as Cr, Mo and Nb in Inconel 625 alloy, a large number of secondary phases may also appear during the cooling process following the hot working (for instance, forging or rolling) [6–8]. Solid solution treatment is often used to further control the morphology, size, quantity and distribution of strengthening phases in the alloy, so as to obtain a good combination of mechanical properties [9, 10]. Therefore, understanding the relationship between the microstructural evolution and mechanical properties is vital for optimizing the treatment parameters and improving mechanical properties of nickel alloys [11–13].

To establish a suitable solution treatment process, Hu et al. [14] prepared Inconel 625 ingots by laser solid forming and investigated the influences of solution treatment temperature on the microstructures and hardness of the samples. The authors concluded that static recrystallization completely in the solution-treated samples at 1200 °C, and the volume fraction and size of Laves phase decreased with the increase in solution treatment temperature. The grain growth was also identified with the increase in solution heat-treating temperature. Liu et al. [15] reported that the grain size of Inconel 625 alloy increased with either raising the temperature or extending the holding time at temperatures above 1050 °C, and the grain growth was controlled by grain boundary diffusion during solution treatment. Several researchers analyzed the relationships between the microstructures and mechanical performances of the Ni-based alloy subjected to the solution treatment. Marchese et al. [16] studied the solution treatment at 1150 °C for 2 h of Inconel 625 alloy manufactured by laser powder bed fusion. The treatment was found to result in recrystallization and grain growth. After aging at 700 °C for 24 h, the grain size remained unchanged, while the precipitation of fine intragranular  $\gamma''$  phases and carbides took place. The alloy strength was improved at the expense of its ductility [17-19]. Giulio [20] discussed the effect of different heat treatment process on the properties of the alloy, including stress relieving treatment at 870 °C for 1 h, annealing treatment at 871-1092 °C for 1 h and solution annealing treatment at 1150 °C for 2 h [21]. They came to a conclusion that stress relieving treatment induce the formation of  $\delta$  phase as well as possible fine carbides; annealing treatment result in the formation of tiny carbides along the grain boundary and fine carbides is detected in the grains; solution annealing treatment reveals the recrystallization, and grain growth with the formation of equiaxed grains and microstructure consists of equiaxed grains and fine submicron carbides. Gao et al. [22] reached similar conclusion; the mechanical properties of the alloy in different states are obtained by sequentially extruding the as-cast samples by hot extrusion, solution treatment, cold rolling and annealing. After cold rolling, although the strength of the alloy is greatly improved, there is more plastic damage. On the contrary, after solution treatment, the alloy obtains relatively high tensile strength while maintaining excellent plasticity. Above all, it can be conclude that the heat treatment process has an important influence on the structure of the alloy, and thus exhibits different mechanical properties.

Although the solution treatment has been studied in an attempt to improve the mechanical properties of Inconel 625 alloy, the role of the treatment temperature in governing the microstructural development and mechanical properties of Inconel 625 alloy remains unclear. The lack of such critical understanding has impeded the design and application of Inconel 625 alloy for engineering applications involving severe conditions. In this paper, the effect of solution treatment temperature was examined on the change of the alloy microstructure and the secondary phase formation in Inconel 625 alloy. The mechanical properties of the alloy corresponding to different treatment temperatures are compared. Finally, the relationship between the solution treatment temperature and microstructure evolution of the hot rolled Inconel 625 alloy was revealed, and the microstructural contribution to the tensile properties of the alloy was discussed.



### Experimental procedure

Inconel 625 alloy was smelted by vacuum induction melting. The ingot was prepared by electroslag remelting (ESR) in protective atmosphere, before being forged with a blooming process, and then hot rolled into 20-mm-thick plate. The chemical composition of the ingot was measured by a direct reading spectrometer (MAXx LMF15, Spectro, Germany), and the measurement results are shown in Table 1.

After cutting and polishing, the sample was covered with anti-oxidation coating before being placed in a resistance furnace under a vacuum of  $5 \times 10^{-2}$  MPa. The solution treatment was undertaken at temperatures of 950 °C, 1000 °C, 1050 °C, 1100 °C and 1150 °C, each for 10 min. Before the microstructure characterization, the specimens were ground successively with silicon carbide abrasive papers of 400-1500 grain size, and then polished with a diamond polishing paste of 2.5 microns. The polished specimens were etched with the solution of  $FeCl_3$  (5 g) + HCl (30 ml), and then rinsed with alcohol before drying. Then, microstructure is observed by BX60M metallographic microscope and FEI Sirion field emission scanning electron microscope (SEM). The electron backscatter diffraction (EBSD) analysis technology is used to characterize texture evolution during solid solution. In order to determine the composition and types of the secondary phase precipitated from hot rolled alloy, the microstructure and structure are observed by Tecnai-G2 transmission electron microscopy (TEM) equipped with energy dispersive spectrometer (EDS). Nano Measurer software is used to measure the average grain size.

All the specimens tested for mechanical properties are proceed by wire electric discharge machine and grinded then polished subsequently. The hardness is tested by FM-700 Vickers hardness tester (Future-tech, Japan) with a load of 500 g, and the full time is maintained for 15 s. The average value of the indenter is obtained at least 7 points per specimen. The tensile tests were conducted at room temperature, tested by CMT5105 (Xinsansi, Shanghai, China) electronic universal tension testing machine.

**Table 1** Chemical compositions of Inconel 625 alloy (mass fraction, %)

| Cr    | Mo   | Nb   | Fe    | С     | Al   | Ti    | Mn    | S      | P      | Ni    |
|-------|------|------|-------|-------|------|-------|-------|--------|--------|-------|
| 20.85 | 8.65 | 3.78 | 0.326 | 0.067 | 0.24 | 0.255 | 0.161 | 0.0035 | 0.0014 | Rest. |

Rectangular dog-bone-shaped specimens were prepared with a gauge dimension of  $20 \times 4 \times 3$  mm<sup>3</sup>. The strain rate was set at  $2 \times 10^{-3}$ /s. The tensile axis was made in parallel with the rolling direction. Three samples are tested in each group representing different processes in order to reduce the error.

### Results and discussion

# Microstructure of hot rolled Inconel 625 alloy

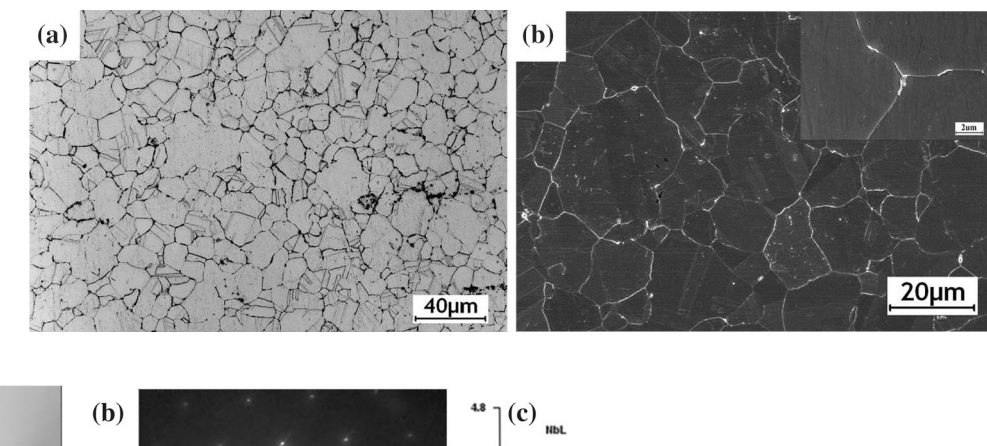
Figure 1 shows the microstructure of hot rolled Inconel 625 alloy. It can be seen that the average grain size is about 15 um. Inconel 625 is mainly composed of austenite ( $\gamma$ ) phase with a large number of twins. There is also a small amount of secondary phase in the alloy, which is irregular in shape and has a size of 0.2–1 um, forming chains at the grain boundaries.

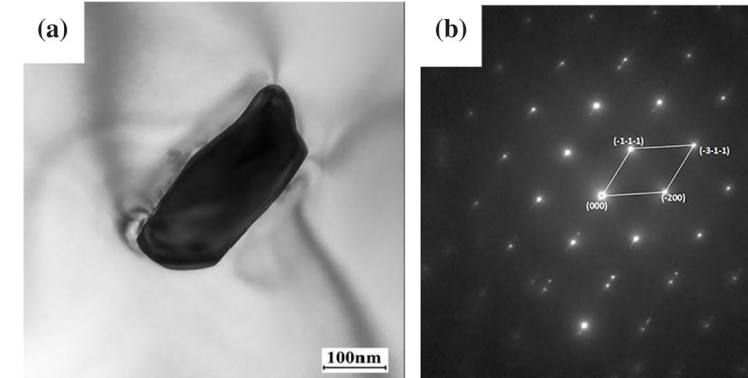
To determine the composition and structure of the secondary phase in hot rolled alloys, selective electron diffraction (SAED) and energy dispersive spectroscopy (EDS) were applied to analyze the secondary phase particles (as shown in Fig. 2). Results showed that the secondary phase is made of MC-type carbide rich in Nb, Mo and C elements. Figure 3 shows that Cr and Ni are uniformly distributed in the matrix, and a minor segregation of Al and Ti elements can be seen in the precipitated phase, while Nb and Mo elements are enriched in the precipitated phase, which is consistent with TEM analysis.

#### Microstructural evolution

As the Inconel 625 samples were held at different temperatures (950, 1000, 1050, 1100, 1150 °C, respectively), each for 10 min, the SEM is shown in Fig. 4, with locally enlarged view placed as inset in the upper right corner. With the increase in solution treatment temperature, the secondary phase chains were found to break up, with the carbide particles gradually decomposing and dissolving. Spheroidization occurred to the large particles which are difficult to dissolve and thus remained in the

Figure 1 Microstructure of hot rolled Inconel 625 alloy: a OM, b SEM.





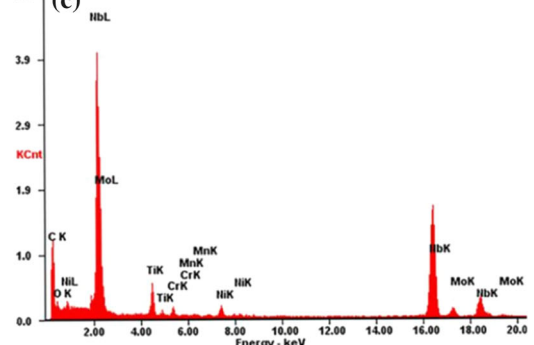
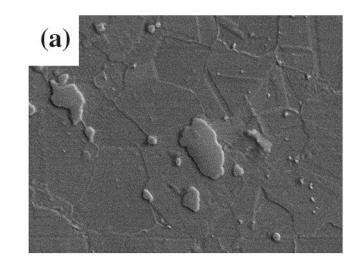
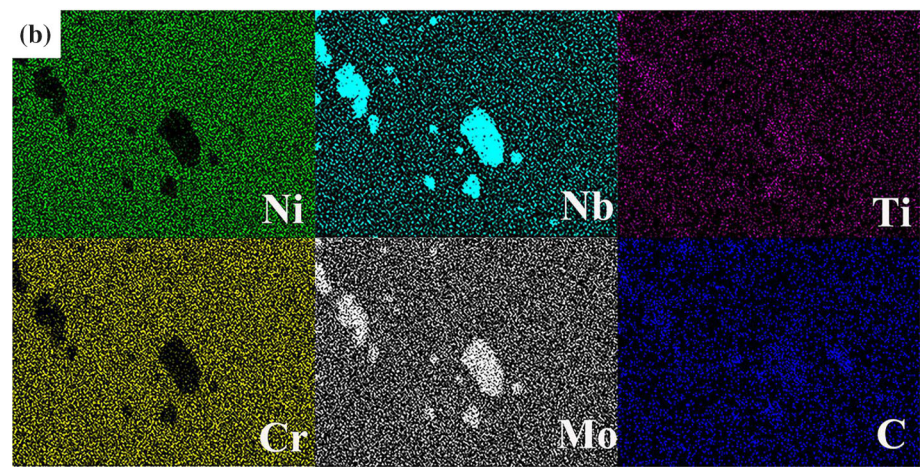


Figure 2 TEM images of carbides in Inconel 625 alloy: a bright field image, b SAED pattern, c EDS.

Figure 3 Element mapping of hot rolled Inconel 625 alloy determined by EDS a SEM, b Mapping of element distribution.



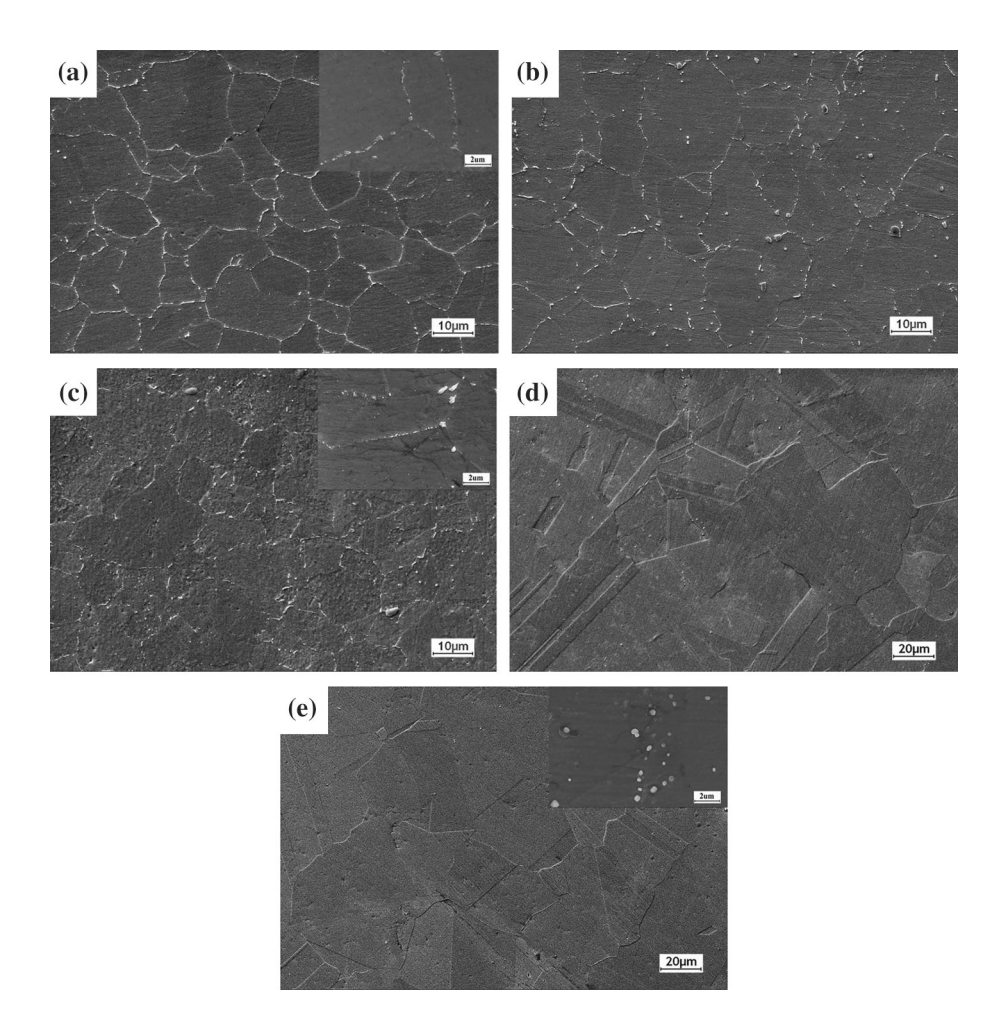


matrix. Apart from that, the average grain size did not change significantly when the solution treatment temperature is 950–1000 °C, which is about

13–16  $\mu m$ , almost unchanged compared with the average grain size of hot rolled alloy of 15  $\mu m$ . When the solution treatment temperature is 1050 °C, the

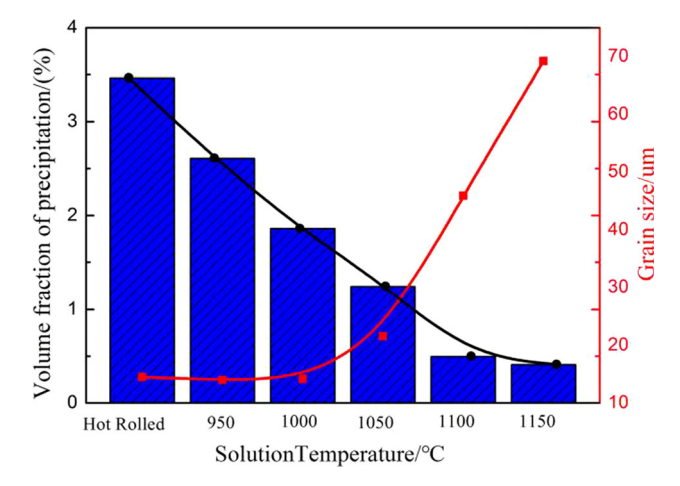


Figure 4 SEM images of Inconel 625 alloy after different heat treatment temperatures a 950 °C, b 1000 °C, c 1050 °C, d 1100 °C, e 1150 °C.



grains grow slightly, and the average grain size is about 19  $\mu m.$  As the temperature rises to 1150 °C, the grains grow sharply, and the average grain size is exceed over 70  $\mu m.$  At the same time, there are still some twins in the austenite structure of Inconel 625 alloy after heat treatment. Some of these twins terminate in the crystal and some cross the whole grain. With the increase in solution treatment temperature, the twin structure does not disappear, but continues to grow with the growth of grains. The variation of volume fraction and grain size of precipitated phase with solution treatment temperature is shown in Fig. 5.

Figure 6 shows the EBSD micrographs of alloys with different solution treatment temperatures. Compared with OM diagrams, EBSD diagrams can clearly show the microstructures and grain boundaries. It can be seen that the grain size of equiaxed grains increases significantly with the increase in heat treatment temperature, and twin interfaces are found in the alloys. This indicates that static

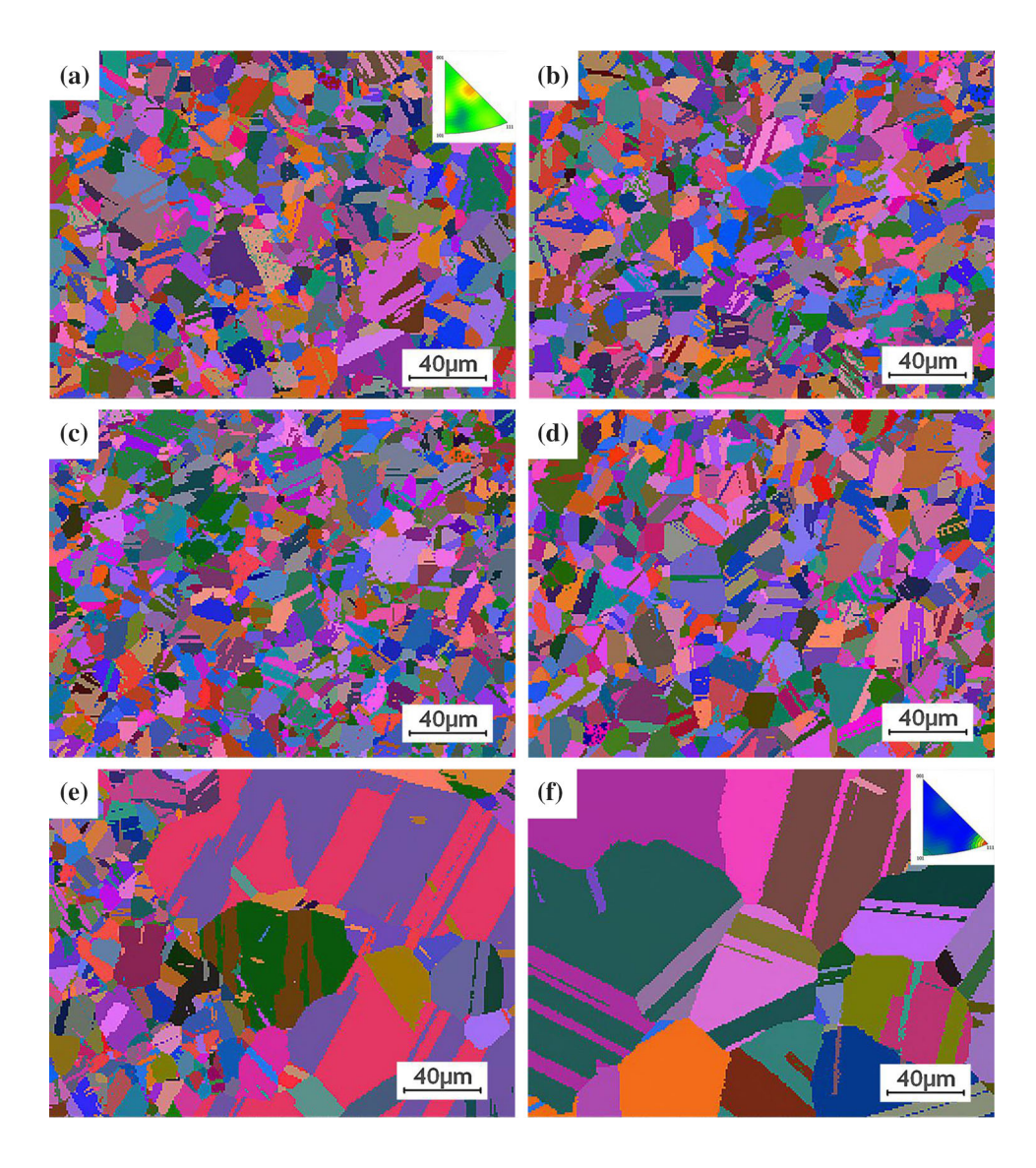


**Figure 5** Volume fraction of precipitation and the grain size of Inconel 625 alloy after different heat treatment temperatures.

recrystallization occurs in solid solution-treated alloys, and dynamic recrystallization occurs in the hot rolled alloys. Mixed crystal structure containing a small amount of fine grains besides large



Figure 6 EBSD maps of the as-deposited sample and after different solution heat treatment samples **a** hot rolled, **b** 950 °C, **c** 1000 °C, **d** 1050 °C, **e** 1100 °C, **f** 1150 °C.



recrystallized grains is shown in Fig. 6e, which makes clear that recrystallization at this time is incomplete compared with heat treatment at 1150 °C. Apart from that, the grain texture distribution of different samples is obtained by EBSD, as shown in Fig. 7. It can be seen that the internal texture intensity of hot rolled alloys is weak, which is related to dynamic recrystallization during hot rolling. However, the <111> texture of the alloy after 1150 °C solution treatment is significantly enhanced, which should be the result of static recrystallization, as shown in the reverse pole diagram signed in the upper right corner of Fig. 6a, f and the pole diagram of Fig. 7a, b.

### Mechanical properties

Figure 8 shows the tensile stress–strain diagram of Inconel 625 alloy after solution treatment at 950–1150 °C. The statistics of changes in mechanical properties, including tensile strength, yield strength, hardness and elongation of Inconel 625 alloy are shown in Fig. 9a–d, respectively.

It can be seen that the elastic modulus of Inconel 625 is about 227 GPa in Fig. 8, and the results are shown in Fig. 9, which demonstrates that the hardness, tensile strength and yield strength of the alloy did not change significantly when the solution treatment temperature is 950–1050 °C. The tensile strength is basically stable at about 940 MPa, the yield strength fluctuate around 455 MPa, and the hardness is stable at about 250 Hv. Similarly, the



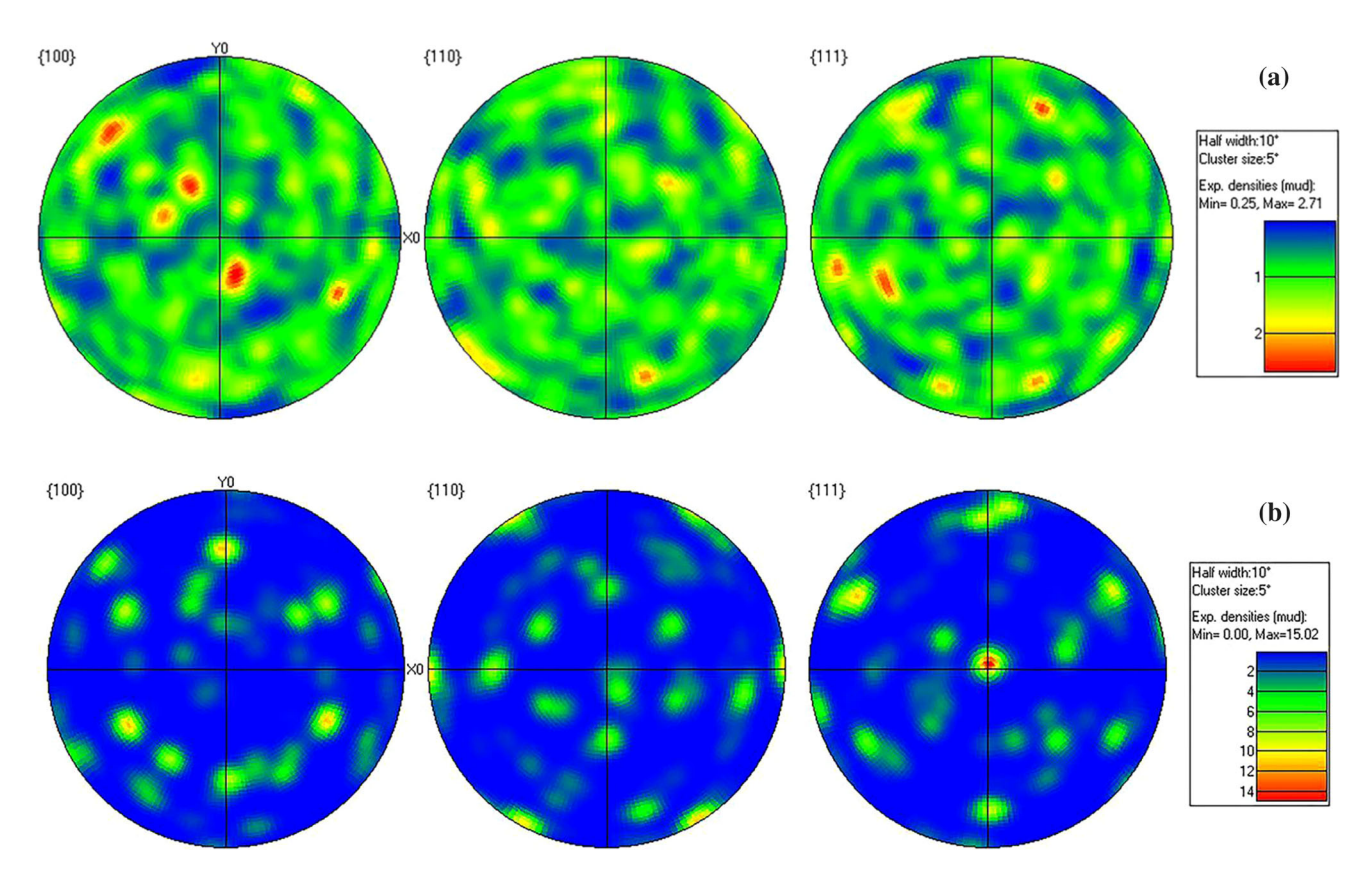


Figure 7 Pole figures of different samples a Hot rolled alloy, b solution treatment temperature at 1150 °C.

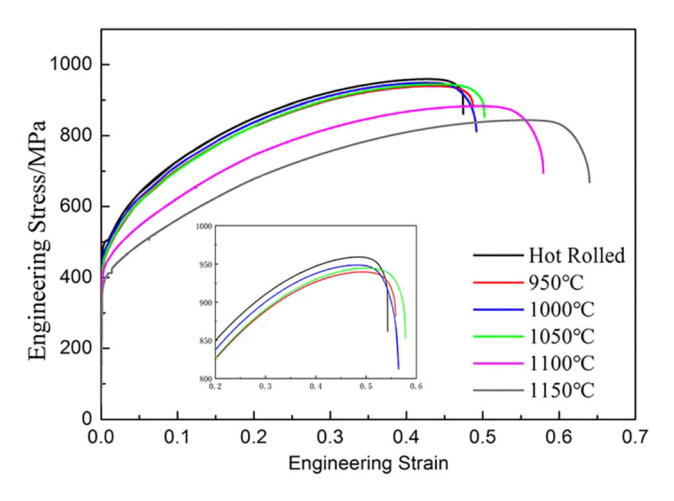


Figure 8 Stress-strain curves of Inconel 625 alloy.

elongation increases slightly with the increase in temperature and reaches 50% at 1050 °C, which is a stroke above that of 47.5% as hot rolled. It can be conclude from Fig. 9, the mechanical properties of Inconel 625 alloy are relatively stable after solution at 950–1050 °C, and the main reasons are synthesized as follows:the average grain size of Inconel 625 alloy does not change much (range from 13 to 16  $\mu$ m), the

carbide dissolution in the alloy is insufficient, and the size of carbides does not reduces significantly.

When the solution treatment temperature rises to 1150 °C, tensile strength of the alloy is about 844 MPa, which is about 12% lower than that of the hot rolled alloy. While the yield strength and hardness gradually decreased, the elongation increased steadily to 64%. Under similar processing conditions, i.e., the hot extruded sample being subjected to a solution treatment at 1150 °C for 1 h, the results showed that the tensile strength was 740 MPa and the elongation to failure was 60% [22]. Additionally, the mechanical properties are comparable with those obtained at 1200 °C for 90 min [23]. This is due to the combined effect of grain size, carbide and twins. Although serious grain size coarsening (average grain size of 74 um) was unfavorable to plasticity, a large number of carbide particles were dissolved during this period, which reduced the weakening effect brought about by carbide particles on the grain boundaries. At the same time, a large number of twin grain boundaries acted to compensate the adverse effects of grain growth and grain boundary



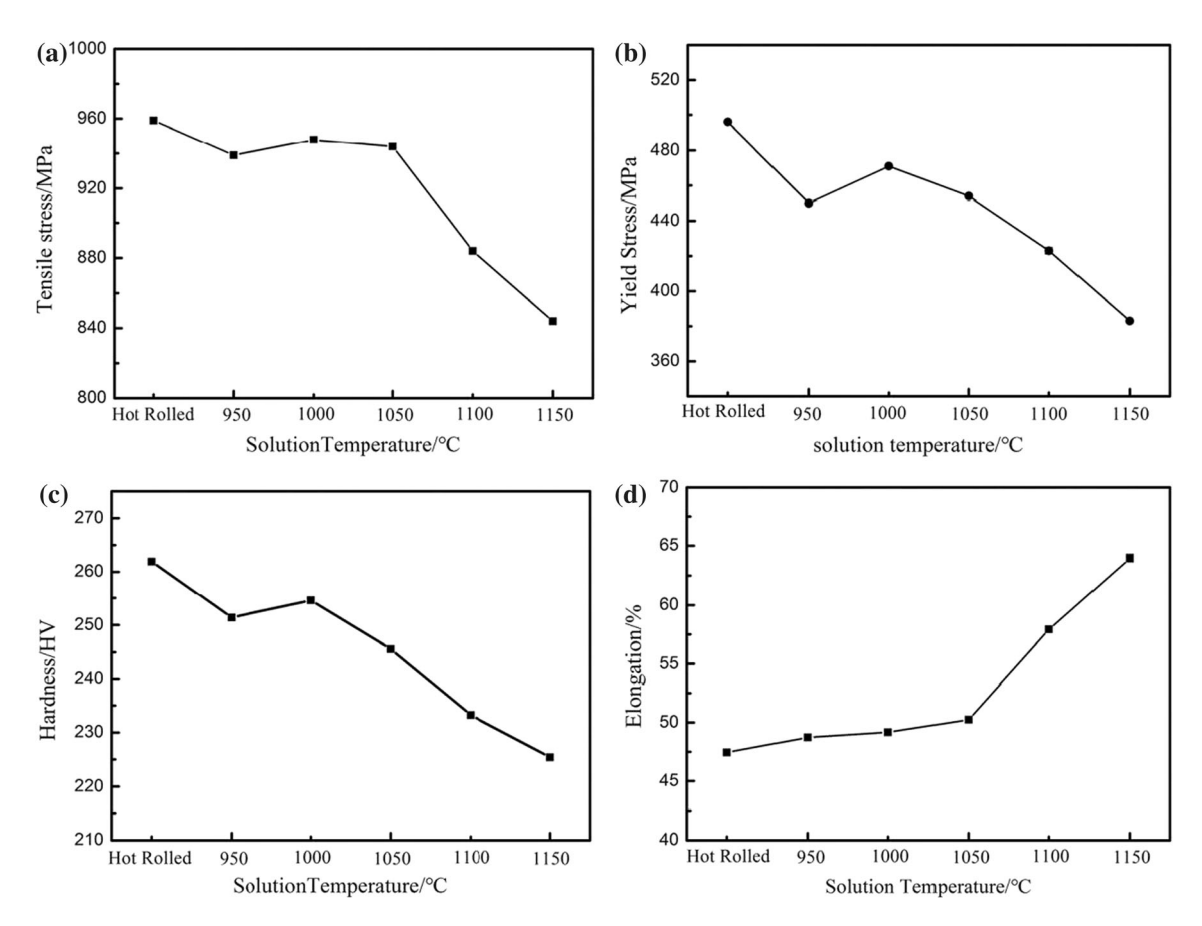


**Figure 9** Mechanical property change of Inconel 625 alloy as a function of different heat treatment temperatures **a** tensile strength, **b** yield strength, **c** hardness, **d** elongation.

migration, and helped lower the probability of stress concentration, thus the overall plasticity was developed.

### Discussion

# Effects of solution treatment temperature on microstructures

After hot rolling, a large number of carbide chains were distributed at the grain boundaries (Fig. 1b). When the solid solution treatment temperature reached 950 °C, a small amount of carbide particles started to dissolve. As the temperature continued to rise, the carbide phase dissolved partially at the grain boundaries with some carbide chains breaking off. When the solution temperature further increased to 1150 °C, the carbide almost disappeared from the grain boundaries, confirmed by the change of the second-phase diffraction peak as shown in Fig. 10. As shown in Fig. 4e, the grains grew rapidly, and only a

small amount of relatively large granular carbide particles (sub-micrometer in size) remain in the matrix. The dissolution rate of carbides is slow when the solution treatment temperature is below 1100 °C, and the dissolution rate of carbides accelerates sharply when the solution treatment temperature rises to 1150 °C, and the carbides in the alloy are almost dissolved. As a hot deformation-induced precipitation strengthening alloy, solution treatment temperature has a great influence on the volume fraction of the secondary phase of the alloy.

The varying grain size and carbide content are the remarkable characteristics of Inconel 625 alloy after solution treatment at different temperature [3]. The grain size of the alloy does not change much when the solution treatment temperature is less than 1100 °C [15]. With the increase in the solution treatment temperature, the chain carbides at the grain boundary gradually break up, and some carbides at the grain boundary gradually dissolve into the matrix [24, 25]. The grain size of the alloy increases rapidly,



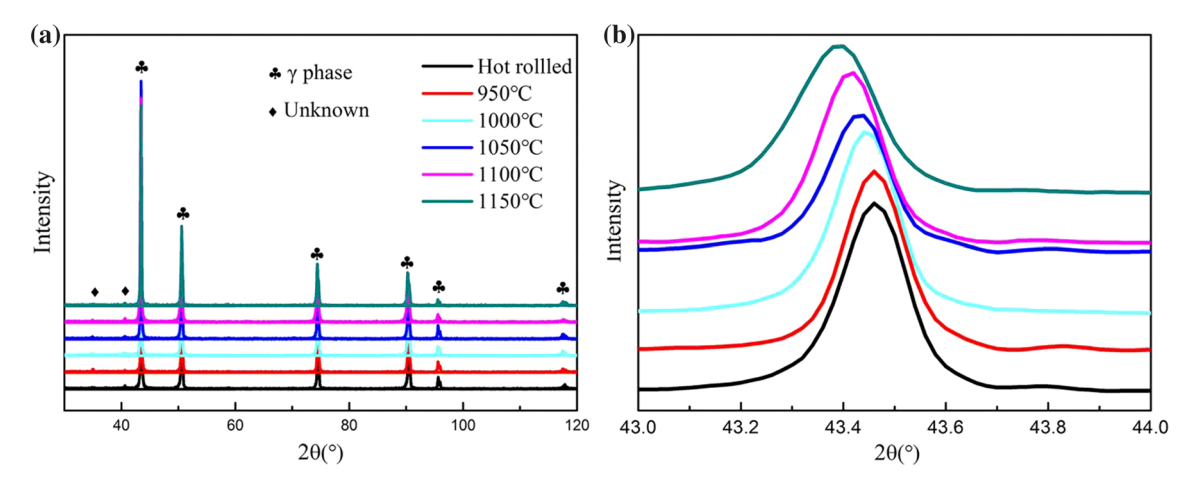


Figure 10 a XRD curve of samples prepared under different treatment conditions, b local amplification of  $2\theta$  (43°-44°).

and the carbides are fully dissolved when the solution treatment temperature reaches 1150 °C [16]. The grain growth is always accompanied by grain boundary migration, which indicates that the grain boundary migration is easier when the solution treatment temperature reaches 1150 °C. On the other hand, carbides as the secondary phase increase the activation energy of grain boundary diffusion that pins the grain boundary and inhibits grain growth [26]. Therefore, when the solution treatment temperature is below 1100 °C, the existences of a large number of secondary phases at the grain boundary prevent grain boundary migration, and the grain size does not change significantly [14], and the morphology of secondary phase changes gradually from chains to dot. It is known to all that the minimum dissolution treatment temperature of MC-type carbides is lower than 1150 °C; as a result, when the solution treatment temperature rises to 1150 °C, the whole carbides are dissolved in the matrix, and the grains size develops rapidly.

# Effects of solution treatment temperature on mechanical properties

The mechanical properties of the material studied in this paper are significantly affected by temperature changes. The mechanical properties change slowly as the heat treatment is carried out below 1050 °C. The strength decreases obviously, and the plasticity increases rapidly when heat treatment is higher than 1100 °C. This phenomenon is discussed in the following chapters from the point of view of strengthening mechanisms.

There are four main strengthening mechanisms that can be used to illustrate the solid solution softening of alloys: refinement strengthening, solid solution strengthening, precipitation strengthening and dislocation strengthening.

### Refinement strengthening

As the most widely discussed strengthening mechanism, refinement strengthening improves the mechanical strength of materials by reducing the average free path of dislocation motion and hindering dislocation motion. The effect of reinforcement can be described by Hall–Petch equation [27, 28].

$$\sigma_r = \sigma_0 + k \cdot d^{-1/2} \tag{1}$$

where  $\sigma_0$  is the lattice frictional stress corresponding to the yield strength of single crystal, and k is the Hall–Petch coefficient; the previous studies [29] have shown that for Ni-based superalloys, the value of k is usually about 750 MPa um<sup>1/2</sup>, and d is the average grain size, attained by intercept method. Therefore, the effect of grain size on the strength of alloys could be expressed by the following formula.

$$\Delta \sigma_r = k d_T^{-1/2} \tag{2}$$

 $d_T$  denote the grain size of alloy solid solution at temperature T. The effect of twin boundary is not considered in the present grain size statistics because of its low volume fraction. According to Eq. (2), the contribution of grain refinement for the tensile strength can be estimated in different states samples. Therefore, there is no doubt that with the continuous increase in solution treatment temperature or the



prolongation of holding time, the grains will continue to grow and the strength of the alloy will decline more obviously.

### Solid solution strengthening

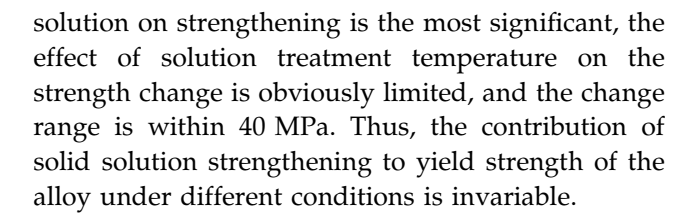
Most of the solid solution strengthening models in traditional alloys are based on binary dilute solid solutions [30, 31]. Figure 10b shows that as the solution treatment temperature rises, the diffraction peak shifts to the left, indicating that the lattice distortion took place in the alloy matrix, caused by the dissolution of a large number of atoms into the matrix. Therefore, the following formulas can be used to characterize the effect of solid solution strengthening [32–34].

$$\Delta \sigma_s = \sum_i K_i \sqrt{C_i} \tag{3}$$

 $K_i$  is the strengthening factor reflecting the strengthening capability of alloying element i. C indicates the molar ratio of elements in the  $\gamma$  matrix. From the analysis of 3.1, it can be seen that the main solid solution elements in the heating process of alloy are Nb and Mo. Arriving from the difficulties to accurately determine trace elements by EDS, to simplify the calculation, all additive elements are considered as one type of solid solution atoms. The statistical results show that the volume fraction of Nb and Mo are the highest, and the strengthening coefficient *K* is obviously higher than other elements. Therefore, only the influence of Nb and Mo is calculated in this statistic, and the comprehensive strengthening factor of  $K_i$  was set as 1100 MPa. The solution elements content in the matrix are listed in Table 2, and the enhancement effect of solution strengthening is shown in Table 3. Although the effect of solid

**Table 2** Content of elements in matrix  $\gamma$  phase and the their relevant solid solution strengthening constants  $K_i(d\sigma/d\sqrt{C_i})$  [31]

| Alloy      | Ni     | Cr     | Nb     | Mo     | Rest   |
|------------|--------|--------|--------|--------|--------|
| Hot rolled | 0.6653 | 0.2434 | 0.0237 | 0.0675 | 1E-04  |
| 950 °C     | 0.6542 | 0.2467 | 0.0238 | 0.0684 | 0.0069 |
| 1000 °C    | 0.6515 | 0.2476 | 0.0242 | 0.0692 | 0.0075 |
| 1050 °C    | 0.6553 | 0.2418 | 0.0254 | 0.0695 | 0.008  |
| 1100 °C    | 0.6416 | 0.2486 | 0.0272 | 0.0788 | 0.0038 |
| 1150 °C    | 0.6446 | 0.2452 | 0.0304 | 0.073  | 0.0068 |
| Ki/MPa     | _      | _      | 1183   | 1015   | _      |



### Precipitation strengthening

The precipitation strengthening mechanism plays a non-negligible role in the alloy. From the perspective of the interaction between dislocations and precipitation phases, the mechanism can be roughly divided into two types: the Orowan-loop mechanism and the particle shear mechanism. Simply put, the bypass mechanism mainly occurs when the secondary phase is large in size or uncoherent with the matrix; in contrast, when the secondary phase is small in size or substantially coherent with the substrate, the particles are cut through. There are many types of precipitated phases in the Inconel 625 alloy system, some of which are non-coherent with the matrix structure and have larger size, which accords with the former. The enhanced contribution of Orowan mechanism is calculated by the following formula [35]:

$$\sigma_{or} = M \cdot 0.4Gb / \left(\pi\sqrt{1-\nu}\right) \cdot \ln(2\overline{r}/b) / L_{S} \tag{4}$$

In the formula, M=3.06 is Taylor factor, G=87 GPa is the shear modulus for the Inconel 625, which is obtained by the formula G=E/2(1+v), with Poisson's ratio v=0.3.  $b=\sqrt{2}\alpha/2$  is the Burger's vector of the total dislocation of the FCC crystal, a is the lattice constant and can be obtained from the XRD analysis in Fig. 10b.  $\overline{r}=\sqrt{2/3}\cdot r$  represents the radius of particles on the slip surface, in which r=1 is the average radius of particles,  $L_S=2\overline{r}(\sqrt{\pi/(4f)}-1)$  is the average spacing of particles, f=1 is the volume fraction of secondary phase particles. Relevant parameters are shown in Fig. 6, and the strengthening increment caused by solid solution strengthening is given in Table 3.

### Dislocation strengthening

Under deformation, the density of intragranular dislocations increases, and the dislocations are prone to cross slip, causing dislocation entanglement, resulting in the obstacles to dislocation motion, leading to plastic deformation continues to be difficult, thereby



**Table 3** Computational results of various strengthening contributions in different specimens for tensile strength

| Alloy      | $\Delta\sigma_{ m r}/{ m MPa}$ | $\Delta\sigma_{ m s}$ /MPa | $\Delta\sigma_{ m or}$ /MPa | $\Delta\sigma_{ m d}/{ m MPa}$ | Δσ/MPa |
|------------|--------------------------------|----------------------------|-----------------------------|--------------------------------|--------|
| Hot rolled | 196.96                         | 332.29                     | 149.02                      | 173.17                         | 851.44 |
| 950 °C     | 200.59                         | 346.32                     | 132.91                      | 143.88                         | 823.70 |
| 1000 °C    | 199.31                         | 349.41                     | 115.99                      | 134.83                         | 799.54 |
| 1050 °C    | 161.49                         | 352.82                     | 110.81                      | 91.99                          | 717.11 |
| 1100 °C    | 110.65                         | 364.45                     | 55.04                       | 61.93                          | 592.07 |
| 1150 °C    | 90.15                          | 366.10                     | 46.45                       | 49.72                          | 552.42 |

increasing the strength of the alloy, which can be expressed by.

$$\Delta \sigma_d = M \beta G b \rho^{1/2} \tag{5}$$

where M is Taylor factor,  $\beta = 0.2$  is a constant for FCC metals, G is the shear modulus,  $\rho$  stands for the dislocation density, and b is the burger vector. We estimate the distribution of dislocations in materials is isotropic, and there is no interaction between dislocations [36], and the dislocation density can be attained by Williamson–Hall method [37], which is a widely used first-order approximation method for evaluating the effects of micro-strain and crystal size [33].

$$\rho = 2\sqrt{3} \cdot \varepsilon / (b \cdot D) \tag{6}$$

$$FWHM \cdot \cos \theta = K\lambda/D + 2\varepsilon \sin \theta \tag{7}$$

where FWHM is the full width at half maximum of the Bragg peaks, K = 0.9 is the coefficient,  $\lambda = 0.154$  Å is the wavelength of the Cu Ka radiation, D is the microcrystalline size,  $\varepsilon$  is the microcrystalline strain, and  $\theta$  is the Bragg angle of the corresponding XRD. According to the XRD values, the parameter  $\varepsilon$  is determined by the slope of the linear fit of the

 $\beta\cos\theta - 2\sin\theta$  and is plotted in Fig. 11a, so as to, the dislocation density is shown in Fig. 11b.

For the sake of clarity, we have summarized a histogram (see Fig. 12) that directly shows the individual contributions and overall contributions of the four enhancement mechanisms. From Table 3 and Fig. 12a, it can be seen that the total strengthening effect of the alloy is larger. According to the analysis of precipitated phase distribution in Fig. 2, the precipitated phase particles are mainly distributed near the grain boundary. Therefore, the precipitation strengthening effect overlaps with the fine grain strengthening effect, resulting in the calculated total strengthening effect value being higher. By comparing the effect of fine grain strengthening with that of precipitation strengthening, a higher value is selected for calculation, and the final total strengthening effect is obtained as shown in Fig. 12b. Taking into account the calculation error and instrument measurement error in the test, the obtained prediction data are consistent well with the overall trend of the experimental values (marked by the dotted line and the solid line).

It can be seen from above that the tensile strength decreases rapidly at the solid solution treatment temperature ascend than 1050 °C, indicating that the

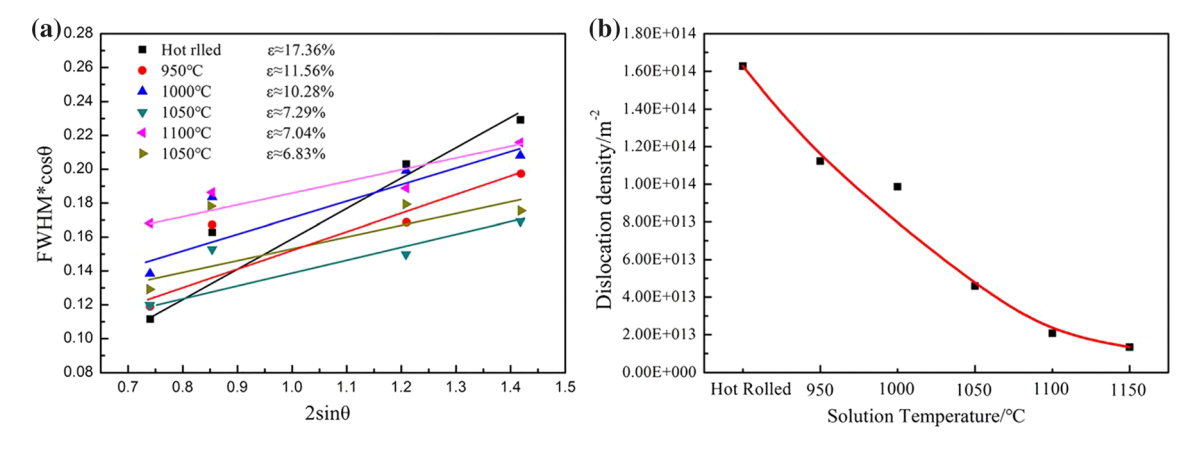


Figure 11 a Micro-strain in different samples, b dislocation density of different samples.



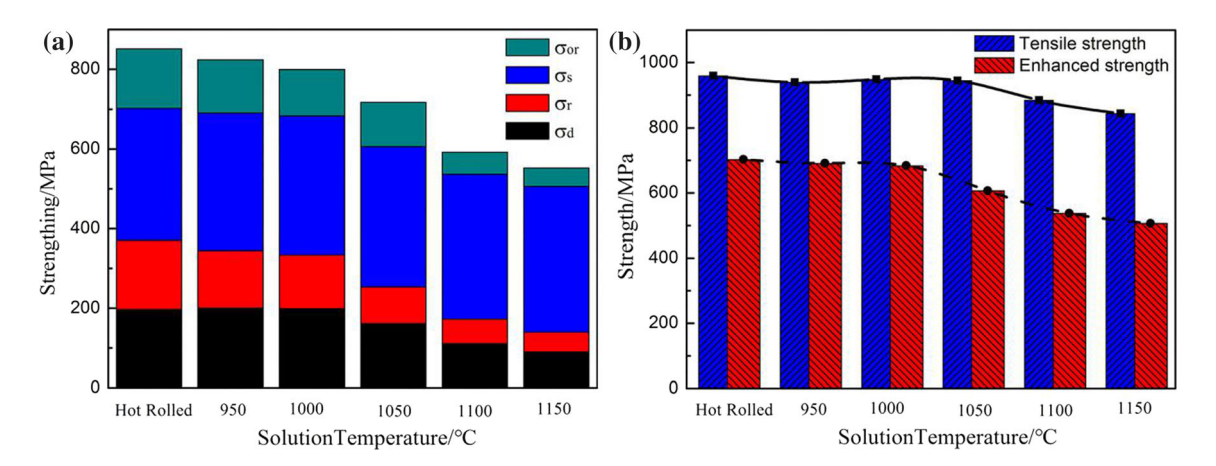


Figure 12 a The strength contributions from different hardening mechanisms, b the calculation values contrast with the experimental data.

recrystallization temperature of the hot rolled 625 alloy is in the range 1050–1100 °C, which agrees well with the EBSD observation. Through comparison, we find that the recrystallization temperature in the hot rolled state is lower than that of the as-cast Inconel 625 alloy [8]. It is believed that deformation storage energy was introduced during the hot rolling process, and the recrystallization driving force is provided during the solution treatment, so that the recrystallization temperature of the alloy was reduced.

### **Conclusions**

The effect of solution treatment temperature on the microstructure evolution and mechanical properties of hot rolled Inconel 625 was studied. The key findings can be summarized as follows:

- 1. The hot rolled Inconel 625 alloy assumes equiaxed FCC austenite structure. The secondary phases are primarily MC carbides rich in Nb and Mo, most of which exist at the grain boundaries in the form of chains. The strength and hardness of hot rolled Inconel 625 alloy are excellent, but the plasticity is relatively weak.
- 2. When the solid solution treatment temperature is 950 °C, a small amount of carbides in the matrix were dissolved at the grain boundaries. As the temperature continues to rise, the carbides on the grain boundaries partially dissolve and the carbide chains are broken up. When the solution treatment temperature was raised to 1150 °C, the chain-like carbides at the grain boundaries

- disappear almost completely, and the grains grow considerably. Only a small number of large granular carbides remain in the matrix.
- 3. After solution treatment at 950–1050 °C, the strength and hardness of the alloy change little, the tensile strength is maintained at 950 MPa, the yield strength is about 460 MPa, the hardness is stable at around 250 HV, and the elongation slightly increases with the increase in temperature. At 1100 °C, it reaches 57.92%, which is about 10% higher than the hot rolled state of 47.45%. When the solution treatment temperature rises to 1150 °C, the tensile strength of the alloy is 844 MPa, which is about 12% lower than that in the hot rolled state. Moreover, the elongation is greatly improved at the expense of the yield strength and hardness.
- There is no plate texture production during the hot rolling, while the <111> recrystallization texture is formed during the solution treatment.
- 5. The theoretical calculation of contributions of various strengthening mechanisms can be used to predict the trend of tensile strength of hot rolled Inconel 625 alloy subjected to solution treatment. With the increase in temperature, the strength of alloy is greatly affected by the variation of grain size and dislocation density.

### Acknowledgements

The work was supported by the Natural Science Foundation of China (51805048), Science and Technology Advancement Program of Jiangsu Province,



China (BA2017112) and the 333 projects of Jiangsu Province, China (BRA2018045). The study was also partly supported by China Postdoctoral Science Foundation funded project (2018M642135) and Key Research Project of Zhangjiagang City, China (ZKG1614). Z Xie acknowledges the support of the Australian Research Council Discovery Projects.

### Compliance with ethical standards

**Conflict of interest** The authors declare that they have no competing financial interests.

## References

- [1] Zhang YC, Jiang W, Tu ST, Zhang XC et al (2018) Experimental investigation and numerical prediction on creep crack growth behavior of the solution treated Inconel 625 superalloy. Eng Fract Mech 199:327–342
- [2] Bakkar A, Ahmed MMZ, Alsaleh NA, Seleman MME-S, Ataya S (2019) Microstructure, wear, and corrosion characterization of high TiC content Inconel 625 matrix composites. J Mater Res Technol 8:1102–1110
- [3] Kim MT, Kim DS, Oh OY et al (2008) Effect of  $\gamma'$  precipitation during hot isostatic pressing on the mechanical property of a nickel-based superalloy. Mater Sci Eng, A 480:218–225
- [4] Dinda GP, Dasgupta AK, Mazumder J et al (2009) Laser aided direct metal deposition of Inconel 625 superalloy: microstructural evolution and thermal stability. Mater Sci Eng A 509:98–104
- [5] Gasson PC (2006) The superalloys: fundamentals and applications R.C.Reed. Cambridge University Press, Cambridge
- [6] Mederios SC, Prasad YVRK, Frazier WG et al (2000) Microstructural modeling of metadynamic recrystallization in hot working of in 718 superalloy. Mater Sci Eng A 293:198–207
- [7] Li DF, Guo QM, Guo SL et al (2011) The microstructure evolution and nucleation mechanisms of dynamic recrystallization in hot-deformed Inconel 625 superalloy. Mater Des 32:696–705
- [8] Kreitcberg A, Brailovski V, Turenne S et al (2017) Effect of heat treatment and hot isostatic pressing on the microstructure and mechanical properties of Inconel 625 alloy processed by laser powder bed fusion. Mater Sci Eng A 689:1–10
- [9] Li S, Wei QS, Shi YS, Zhu ZC, Zhang DQ et al (2015) Microstructure characteristics of inconel 625 superalloy

- manufactured by selective laser melting. J Mater Sci Technol 31:946–952
- [10] Krell J, Röttger A, Theisen W et al (2019) Chromiumnickel-alloys for wear application at elevated temperature. Wear 432–433:102924
- [11] Wang XQ, Carter LN, Pang B et al (2017) Microstructure and yield strength of SLM-fabricated CM247LC Ni-Superalloy. Acta Mater 128:87–95
- [12] Mironenko VN, Aronin AS, Vasenev VV et al (2016) Structure and fracture mechanism of a two-phase chromium– nickel alloy during high-temperature deformation. Phys Met Metallogr 117:937–944
- [13] Semiatin SL, McClary KE, Rollett AD et al (2012) Microstructure evolution during supersolvus heat treatment of a powder metallurgy nickel-base superalloy. Metall Mater Trans A 43:1649–1661
- [14] Hu YL, Zhang SY, Jiang YM, Liu XF et al (2018) Effect of solution heat treatment on the microstructure and mechanical properties of Inconel 625 superalloy fabricated by laser solid forming. J Alloys Compd 767:330–344
- [15] Liu M, Zheng WJ, Xiang JZ et al (2016) Grain growth behavior of inconel 625 superalloy. J Iron Steel Res Int 23:1111-1118
- [16] Marchese G, Lorusso M, Parizia S, Bassini E et al (2018) Influence of heat treatments on microstructure evolution and mechanical properties of Inconel 625 processed by laser powder bed fusion. Mater Sci Eng A 729:64–75
- [17] Zhang DY, Niu W, Cao XY et al (2015) Effect of standard heat treatment on the microstructure and mechanical properties of selective laser melting manufactured Inconel 718 superalloy. Mater Sci Eng A 644:32–40
- [18] Kreitcberg A, Brailovski V, Turenne S (2017) Elevated temperature mechanical behavior of IN625 alloy processed by laser powder-bed fusion. Mater Sci Eng A 700:540–553
- [19] Acharya R, Sharon JA, Staroselsky A (2017) Prediction of microstructure in laser powder bed fusion process. Acta Mater 124:360–371
- [20] Marchese G, Parizia S, Rashidi M (2019) The role of texturing and microstructure evolution on the tensile behavior of heat-treated Inconel 625 produced via laser powder bed fusion. Mater Sci Eng A 767:13850
- [21] Chandler H (ed) (1996) Heat treater's guide: practices and procedures for nonferrous alloys. ASM International, Materials Park
- [22] Gao Yubi, Ding Yutian, Chen Jianjun (2019) Effect of twin boundaries on the microstructure and mechanical properties of Inconel 625 alloy. Mater Sci Eng A 767:138361
- [23] Hu YL, Li YL, Zhang SY (2019) Effect of solution treatment temperature on static recrystallization and ductility of



- Inconel 625 superalloy fabricated by directed energy deposition. Mater Sci Eng A 772:138711
- [24] Divya VD, Muñoz MR, Messé OMDM et al (2016) Microstructure of selective laser melted CM247LC nickelbased superalloy and its evolution through heat treatment. Mater Charact 114:62–74
- [25] Xu FJ, Lv YH, Liu YX et al (2013) Effect of heat treatment on microstructure and mechanical properties of inconel 625 alloy fabricated by pulsed plasma arc deposition. Mater Des 50:48-54
- [26] Wang P, Zhang BC, Tan CC et al (2016) Microstructural characteristics and mechanical properties of carbon nanotube reinforced Inconel 625 parts fabricated by selective laser melting. Mater Des 112:290–299
- [27] Sylwestrowicz W, Hall EO (2002) The deformation and ageing of mild steel: III discussion of results. Proc Phys Soc 64:495
- [28] Fu MW, Chan WL (2014) Size effects in micro-scaled plastic. Springer, London
- [29] Kozar RW, Suzuki A, Milligan WW et al (2009) Strengthening mechanisms in polycrystalline multimodal nickel-base superalloys. Metall Mater Trans A 40:1588–1603
- [30] Fleischer RL et al (1963) Substitutional solution hardening. Acta Metall Sin 11:203–209

- [31] Roth HA, Davis CL, Thomson RC (1997) Modeling solid solution strengthening in nickel alloys. Metall Mater Trans A 28:1329–1335
- [32] Schuh CA, Nieh TG, Iisaki H (2003) The effect of solid solution W additions on the mechanical properties of nanocrystalline Ni. Acta Mater 51:431–443
- [33] He JY, Wang H, Huang HL et al (2016) A precipitationhardened high-entropy alloy with outstanding tensile properties. Acta Mater 102:187–196
- [34] Pouranvari M et al (2015) Solid solution strengthening of transient liquid phase bonded nickel based superalloy. Mater Sci Technol 31:1773–1780
- [35] Argon AS, Bikerman JJ (1971) Physics of strength and plasticity. Phys Today 24:60
- [36] Williamson GK, Hall WH (1953) X-ray line broadening from filed aluminium and wolfram. Acta Metall Sin 1:22–31
- [37] Williamson GK, Smallman RE (1956) III. Dislocation densities in some annealed and cold-worked metals from measurements on the X-ray debye-scherrer spectrum. Philos Mag 1:34–46

**Publisher's Note** Springer Nature remains neutral with regard to jurisdictional claims in published maps and institutional affiliations.



### Terms and Conditions

Springer Nature journal content, brought to you courtesy of Springer Nature Customer Service Center GmbH ("Springer Nature").

Springer Nature supports a reasonable amount of sharing of research papers by authors, subscribers and authorised users ("Users"), for small-scale personal, non-commercial use provided that all copyright, trade and service marks and other proprietary notices are maintained. By accessing, sharing, receiving or otherwise using the Springer Nature journal content you agree to these terms of use ("Terms"). For these purposes, Springer Nature considers academic use (by researchers and students) to be non-commercial.

These Terms are supplementary and will apply in addition to any applicable website terms and conditions, a relevant site licence or a personal subscription. These Terms will prevail over any conflict or ambiguity with regards to the relevant terms, a site licence or a personal subscription (to the extent of the conflict or ambiguity only). For Creative Commons-licensed articles, the terms of the Creative Commons license used will apply.

We collect and use personal data to provide access to the Springer Nature journal content. We may also use these personal data internally within ResearchGate and Springer Nature and as agreed share it, in an anonymised way, for purposes of tracking, analysis and reporting. We will not otherwise disclose your personal data outside the ResearchGate or the Springer Nature group of companies unless we have your permission as detailed in the Privacy Policy.

While Users may use the Springer Nature journal content for small scale, personal non-commercial use, it is important to note that Users may not:

- 1. use such content for the purpose of providing other users with access on a regular or large scale basis or as a means to circumvent access control:
- 2. use such content where to do so would be considered a criminal or statutory offence in any jurisdiction, or gives rise to civil liability, or is otherwise unlawful:
- 3. falsely or misleadingly imply or suggest endorsement, approval, sponsorship, or association unless explicitly agreed to by Springer Nature in writing:
- 4. use bots or other automated methods to access the content or redirect messages
- 5. override any security feature or exclusionary protocol; or
- 6. share the content in order to create substitute for Springer Nature products or services or a systematic database of Springer Nature journal content

In line with the restriction against commercial use, Springer Nature does not permit the creation of a product or service that creates revenue, royalties, rent or income from our content or its inclusion as part of a paid for service or for other commercial gain. Springer Nature journal content cannot be used for inter-library loans and librarians may not upload Springer Nature journal content on a large scale into their, or any other, institutional repository.

These terms of use are reviewed regularly and may be amended at any time. Springer Nature is not obligated to publish any information or content on this website and may remove it or features or functionality at our sole discretion, at any time with or without notice. Springer Nature may revoke this licence to you at any time and remove access to any copies of the Springer Nature journal content which have been saved.

To the fullest extent permitted by law, Springer Nature makes no warranties, representations or guarantees to Users, either express or implied with respect to the Springer nature journal content and all parties disclaim and waive any implied warranties or warranties imposed by law, including merchantability or fitness for any particular purpose.

Please note that these rights do not automatically extend to content, data or other material published by Springer Nature that may be licensed from third parties.

If you would like to use or distribute our Springer Nature journal content to a wider audience or on a regular basis or in any other manner not expressly permitted by these Terms, please contact Springer Nature at

 $\underline{onlineservice@springernature.com}$